Korean J. Chem. Eng., 37(5), 866-874 (2020)
DOI: 10.1007/s11814-020-0497-2

pISSN: 0256-1115
eISSN: 1975-7220

Tailoring the separation performance and antifouling property of polyethersulfone based NF membrane by incorporating hydrophilic CuO nanoparticles

Sayed Mohsen Hosseini*,†, Fatemeh Karami*, Samaneh Koudzari Farahani*, Samaneh Bandehali*, Jiangnan Shen,†, Ehsan Bagheripour*, and Amin Seidypoor***

*Department of Chemical Engineering, Faculty of Engineering, Arak University, Arak 38156-8-8349, Iran
**Center for Membrane Separation and Water Science & Technology, Ocean College,
Zhejiang University of Technology, Hangzhou 310014, China
(*Received 28 November 2019 • accepted 18 January 2020*)

Abstract−CuO/PES composite membranes were fabricated through phase inversion method, focusing on fouling reduction and improving separation performance. Copper oxide nanoparticles were used as filler additive in the membrane structure. The effect of the embedded CuO nanoparticles on the morphology was studied by considering SEM, SOM and 3D surface images. Flux recovery ratio (FRR%), water contact angle, water content, mechanical tensile strength, porosity and mean pore size, salt rejection and water flux were investigated to evaluate the performance of fabricated membranes. The SOM images showed a uniform surface for the modified membranes. SEM images showed a finger-like structure for the modified membranes. Results also denoted an increment in porosity and mean pore size of membrane at low concentration of CuO NPs, whereas the opposite trend was found at higher concentration of nanoparticles. Utilizing CuO NPs enhanced the membrane tensile strength obviously. PWF significantly was improved by applying CuO NPs in membrane matrix. Highest PWF (42.63 L/m^{2}h) was observed for PES-0.05 wt% CuO blended membrane, whereas it was 10.41 (L/m^{2}h) for pristine ones. Salt rejection also measured 82% for virgin membrane and 63-90% for modified membranes. Moreover, FRR% were measured (~77% to ~93%), while the pristine membrane showed ~63% FRR%.

Keywords: Nanofiltration, Hydrophilic Copper Oxide Nanoparticles, Flux Enhancement, Promoted Antifouling Characteristic, Physico-chemical Properties

INTRODUCTION

Membrane separation processes have gained much attention in different domains due to appropriate separation performance and easy operation [1,2]. Also, the ease of fabrication and their low energy consumption make them attractive compared to conventional methods [3-5]. Pressure-driven membranes have been applied widely in desalination and wastewater treatment [6,7]. They are classified to reverse osmosis (RO), microfiltration (MF), ultrafiltration (UF), and nanofiltration (NF) [8-10]. Among these methods, the application of NF membranes is increasing notably in water treatment due to low operation pressure, low maintenance costs, excellent multivalent salt retention, and high flux [11]. Most polymeric materials for NF membrane preparation are cellulose acetate (CA), polyamides (PA), polyvinylidene fluoride (PVDF), polysulfone (PSF), polyvinyl alcohol (PVA), polyimide (PI), and polyethersulfone (PES) [12,13]. Among them, PES is attractive for construction of NF membranes because it shows significant mechanical strength and high thermal stability, high resistance in alkaline and acidic environment, and oxidative properties [14-16]. However, PES membranes have some challenges that limit their application such as their hydrophobic features and the sedimentation and adsorption of large contaminants on the membrane surface and, therefore, low flux and insignificant antifouling properties [17-19].

Fouling phenomenon is one of the major challenges for NF polymeric membranes that reduces separation performance. The studies showed that fouling phenomena can be controlled by the improvement of membrane surface hydrophilicity, decreasing membrane surface roughness. Therefore, most researches considered the polymeric membrane modification by several methods to develop the resistance of fouling and separation performance [20,21].

The techniques for the development of high-performance membranes with excellent antifouling properties are grafting, coating, incorporating of hydrophilic NPs or organic materials. Among the aforementioned techniques, blending with hydrophilic nanomaterials and preparation of mixed matrix membranes (MMMs) is the simple procedure for membrane fabrication [18,22,23]. Most NPs in MMM preparation are metal and metal oxide NPs, carbon-based nanomaterials, carbon nanotubes, multi-walled carbon nanotubes, zeolites, boehmite, and organic NPs including chitosan, and cellulose acetate [24-28]. Introducing nanoparticles into the membrane structure leads to change membrane morphology and separation performance because of the large surface area, small size and good interaction with membrane matrix [29,30]. Metals and metal oxides-based nanoparticles such as ZnO, TiO_2, Fe_3O_4, CuO, Cu and Ag are popular nanomaterials for fabrication of NF membranes because of good antibacterial and antifouling properties [31,32]. The studies show a high potential of metal and metal oxide NPs in waste-

†To whom correspondence should be addressed.
E-mail: s-hosseini@araku.ac.ir, shenjn@zjut.edu.cn

water treatment. Kusworoa et al. [30] synthesized and evaluated nano-hybrid of SiO_2/ZnO-containing PES membranes. The results showed an increase of PWF about 200%, the salt rejection improved 16-18% and the fouling resistance of the membranes increased significantly. Monaheng et al. [33] prepared the PES-based membranes by incorporation of Fe-Ag/functionalized-multiwalled carbon nanotube. The evaluation of membrane performance showed that by addition of hybrid NPs into the membrane, PWF increases from 26.5 in pristine membrane to 36.9 L/m^{2}h in 1 wt% NPs and Cr^{6+} rejection improves up to 94%. Moreover, the presence of Fe-Ag/f-MWCNTs, enhanced fouling resistance of the hybrid membranes. Ahmad et al. [29] investigated the changes of fouling properties of prepared membranes by introducing different concentrations of ZnO NPs into PES/ZnO hollow fiber MMMs. The results demonstrated the progress in fouling resistance, the increment of surface hydrophilicity and surface charge of modified membranes. Hosseini et al. [34] investigated the separation performance of MMMs by introducing Fe_3O_4-polyvinylpyrrolidone into the PES as a membrane matrix. Incorporation of 2 wt% nanoparticles reduced the contact angle from 65.18° for the neat membrane to 50.5°. The PWF increased to 9.96 (L/m^{2}h) in 0.5 wt% NPs. Moreover, the rejection of salt ions was enhanced to 90%. The nanocomposite membrane revealed outstanding antifouling properties.

The application of ZnO nanorods for preparation of NF membranes was reported by Rajabi et al. [18]. The antifouling properties significantly enhanced in 0.1 wt% ZnO NPs. These membranes showed high porosity, hydrophilicity, and PWF compared with neat PES membrane. Madaeni et al. [35] prepared polyacrylic acid (PAA)-functionalized TiO_2 NPs by grafting NPs to the membrane surface. The grafting NPs enhanced the uniform dispersion of nanoparticles and reduced the agglomeration of nanoparticle on the membrane surface. These membranes showed excellent stability during long-term operation due to chemical bonds between TiO_2 and PAA. Copper oxide (CuO) NPs are metal oxide nano-structures that have been applied in gas sensors, photoconductive and photothermal applications, industrial wastewater treatment, solar energy, high-tech superconductors, and catalysts. This is due to the special properties of copper NPs such as good hydrophilicity, proper chemical and physical stability, high surface area, and good mechanical strength [12,36]. The fabricated CuO-containing membranes for water treatment determined the capacity of CuO NPs in this field. Copper oxide (CuO)/PES UF membranes were fabricated by Nasrollahi et al. [29]. The optimized membrane showed the enhancement of hydrophilicity and PWF and antifouling properties.

Nasrollahi et al. [12] studied the effect of doping the NH_2-functionalized CuO (FCN) and ZnO (FZN) NPs on the PES UF membranes. These membranes exhibited considerable enhancement in analyses of permeation and fouling. Hosseini et al. [37] synthesized the barium ferrite/CuO composite NPs in the combination with polyvinylchloride for the fabrication of heterogeneous ion exchange membranes. The modified membranes showed the improvement of electrochemical and antibacterial characteristics. Furthermore, these membranes had a good performance in the removal of E-coli bacteria.

There are few studies on separation performance in CuO-containing NF membranes. Therefore, in this study, the effect of different loadings of CuO NPs was investigated on the separation performance, physico-chemical properties, and the potential of antifouling in PES-based NF membranes. It is expected that due to the interactions between the polymer and copper oxide nanoparticles with regards to their inherent features, the properties of membranes will be particularly affected in the hydrophilicity, the antifouling property, and the flux. The membrane morphology was characterized by SEM, SOM and 3D surface images. Moreover, the separation performance of PES/CuO membranes was investigated by water content, contact angle, porosity, mean pore size, tensile strength, PWF, salt rejection, and the filtration of BSA solution.

MATERIALS AND METHOD

1. Materials

Polyethersulfone (PES, E6020P, M_w: 58,000) was purchased from BASF Co. (New Jersey, USA). Polyvinylpyrrolidone (PVP, M_w: 25,000) as a pore former and N,N-dimethyl acetamide (DMAc, M_w: 87.12) as solvent were supplied from Merck Inc., Germany. Copper oxide nanoparticles (CuO nanopowder, 99%, 40 nm average particle size) were provided by US Research Nanomaterials, Inc., Houston, USA. Sodium sulfate (Na_2SO_4, M_w: 142.04) was prepared from Merck Inc., Germany. Furthermore, deionized water was applied throughout the experiments.

2. Membrane Fabrication

All samples of the membrane were prepared using the phase inversion method. Combination of casting solutions was PES (18 wt%), PVP (1 wt%), DMAC and different concentration of CuO NPs (0, 0.05, 0.1, 0.5, 1 and 2 wt%). The polymeric solutions were stirred by mechanical stirrer at 350 rpm (model: Velp Scientifica Multi 6 stirrer) and at room temperature (25 °C). Afterward, samples were placed in the ultrasonic bath for 1 h for better dispersing and breaking up agglomeration of nanoparticles. For removing the air bubbles completely, the fabricated solutions remained for 24 h without any stirring. Then, the homogeneous solution was cast by an applicator with 150 μm thickness. The precipitation process was done by immersing fabricated membranes in a water bath. The fabricated membranes were placed into the deionized water for 24 h for complete phase inversion process. Table 1 presents the polymeric solution compositions.

3. Membrane Characterization

3-1. Morphological Studies

Scanning optical microscopy (SOM, Olympus model IX 70, in transmission mode) and scanning electron microscopy (SEM, Seron Technology Inc. Korea) were applied to morphological study of pre-

Table 1. The details of composition for fabrication NF membranes

Sample no.	PES (wt%)	PVP (wt%)	DMAc (wt%)	CuO (wt%)
M1	18	1	81.00	0.00
M2	18	1	80.95	0.05
M3	18	1	80.90	0.10
M4	18	1	80.50	0.50
M5	18	1	80.00	1.00
M6	18	1	79.00	2.00

pared membranes. Furthermore, 3D surface image metrology software was used for membrane characterization.

3-2. Water Content

The difference between dry and wet weight for membranes was used to determine membrane water content by the following Eq. (1). For obtaining the dry and wet weight, membranes were measured and then dried in an oven at 80 °C for 12 h [7]:

$$\text{Water content} = \left(\frac{W_w - W_d}{W_w}\right) \times 100 \quad (1)$$

where W_{wet} and W_{dry} refer to the wet and dry weight of prepared membranes, respectively.

3-3. Water Contact Angle

Water contact angle analyzer was applied to characterize the surface hydrophilicity of membranes by deionized water as a probe liquid. Three different locations were considered for determination water contact angle of samples for minimization of experimental errors and the average of values was reported [38].

3-4. Porosity and Mean Pore Size of Membrane

Eq. (2) was considered to obtain porosity (ε) of fabricated membranes [39,40]:

$$\varepsilon(\%) = \left(\frac{W_w - W_d}{\rho_f V_m}\right) \times 100 \quad (2)$$

where W_w and W_d are wet and dry weight (g), ρ_f is water density (g/cm^3) and V_m is membrane volume (cm^3), respectively.

Additionally, the Guerout-Elford-Ferry Eq. (3) was applied to calculate mean pore size (r_m) for all fabricated membranes [41]:

$$r_m = \sqrt{\frac{(2.9 - 1.75\varepsilon)8\eta LQ}{\varepsilon A \Delta p}} \quad (3)$$

where η (8.9×10^{-4} Pa·s) is the water viscosity, l is the thickness of membrane (m), Q is the filtrated pure water flow rate (m^3/s), and Δp is the operating pressure (4.5 MPa).

3-5. Mechanical Strength

ASTM1922-03 was used for the characterization of tensile stress of membranes. The size of samples was 15 mm×80 mm. To reduce the experimental errors, the measurements were repeated three times and then their mean values were reported [34,42].

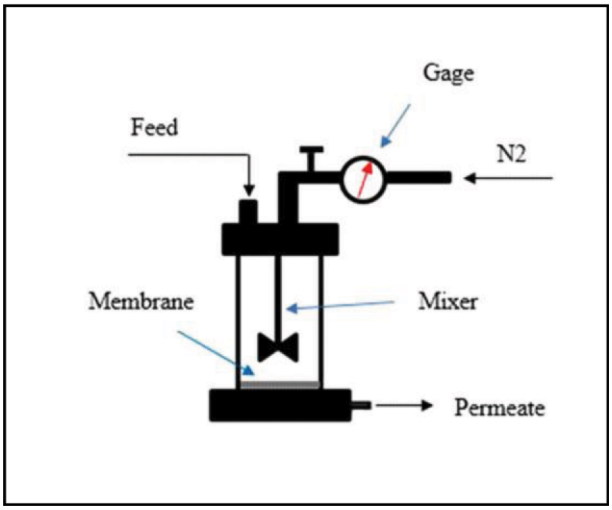

Fig. 1. The schematic diagram of the separation system.

3-6. Membrane Filtration Performance

The filtration test was carried out by a homemade dead-end filtration system. The effective area of filtration system was 11.94 cm^2 as shown in Fig. 1. The compaction of membranes was done before the filtration test by deionized water at 5 bar.

The PWF of NF membranes was obtained by Eq. (4) and measuring the permeated water through the membranes [43-45]:

$$J = \frac{V}{A\Delta T} \quad (4)$$

where J is permeation flux (L/m^{2}h), V is the volume of permeated flux (L), A is the membrane area (m^2) and Δt is time (h). All experiments were done at 25 °C.

The separation performance of NF membranes was calculated by Eq. (5). Na_2SO_4 with the concentration of 1 g/L was considered to determine the membrane ability in salt removal.

$$R\% = \left(1 - \frac{C_p}{C_f}\right) \times 100 \quad (5)$$

where R is membrane rejection, C_f is salt concentration in feed and C_p is salt concentration in permeate. The fouling resistance of membranes was also investigated by flux recovery ratio (FRR%), which was estimated by Eq. (6). For the purpose, after 90 min the primary filtration test of pure water ($J_{w,1}$ (L/m^{2}h)), the powder milk solution as a typical powerful foulant with the concentration of 8,000 mg/L was applied to filtration for 90 min at 4.5 Mpa. Then fouled membranes were placed into the deionized water bath for 1 h at 25 °C and washed with distilled water. Then the PWF was measured again for washed membranes ($J_{w,2}$ (L/m^{2}h)) [41]:

$$FRR(\%) = \left(\frac{J_{w,2}}{J_{w,1}}\right) \times 100 \quad (6)$$

RESULTS AND DISCUSSION

1. Membrane Morphology

Fig. 2 illustrates the cross-sectional SEM images of the pristine membrane (M1) and MMMs (M2 to M6). By introducing of CuO NPs into the polymeric solution, the morphology of membranes changes. All membranes, with and without CuO NPs, revealed a porous and finger-like structure with a dense layer on the top of porous layer; that is confirmation of producing an asymmetric structure in fabricated membranes during the phase inversion process. The top layer or active layer acts as a selective layer and its thickness affects the separation process. The porous layer is known as a support layer. This morphology is related to the rate of exchange between solvent and water (non-solvent) in the phase inversion process and greatly related to kinetic and thermodynamics properties. The hydrophilicity of CuO NPs improves the mass transfer between solvent and water, which leads to forming larger pores and longer channels. As is clear in Fig. 2, by increasing the hydrophilic CuO NPs, the MMMs show larger pores. Moreover, it was found that the volume of macro-voids in MMMs is larger than pristine PES membrane. The polymer solution viscosity is low in

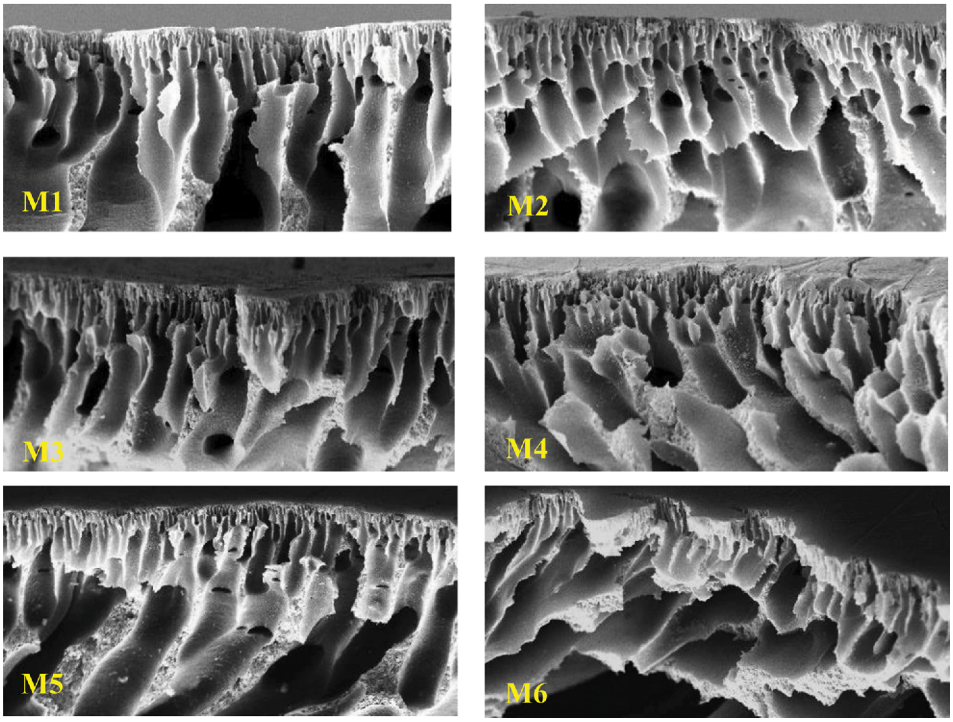

Fig. 2. The cross-sectional SEM images of prepared membranes: Pristrne mebrane (M1) and mixed matrix membranes in different concentration of CuO nanoparticles (M2 to M6).

low concentrations of nanoparticles (0.05 to 0.1 wt%). Therefore, rapid demixing occurs between solvent and water because of the good affinity of CuO NPs with water molecules, which leads to higher pores into the membrane structure [46-48]. The SEM images confirm the larger cavities and longer finger-like structure in low concentration of CuO NPs. But at high concentration of copper oxide NPs (2 wt%) grow the viscosity of casting solution leading to delay the rate of water-solvent exchange, which creates small cavities. Moreover, nanoparticles migrate to the membrane surface and

Table 2. The porosity and mean pore size of all fabricated membranes

Membrane	Porosity (%)	Mean pore size (nm)
M1-pristine membrane	68	44.48
M2-0.05 wt% NP	74	81.0
M3-0.1 wt% NP	76	85.07
M4-0.5 wt% NP	70	90.84
M5-1 wt% NP	67	73.57
M6-2 wt% NP	64	71.02

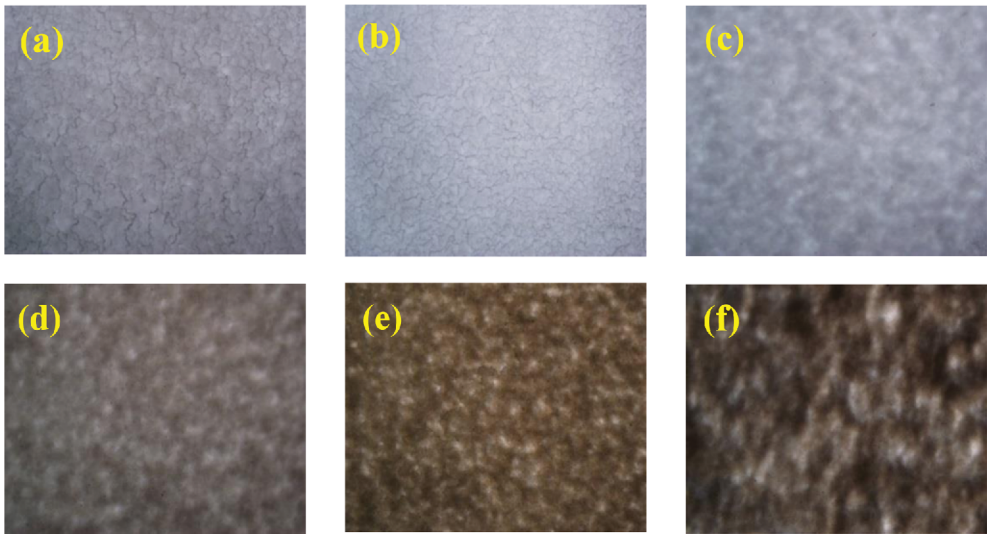

Fig. 3. The SOM images (10X magnifications) of prepared membranes with different concentrations of CuO nanoparticles.

increase the selective layer thickness [42,49]. As shown in Fig. 2, M6 shows the highest selective layer thickness. By migration of nanoparticle to the membrane surface, the possible agglomeration of CuO NPs on the surface increases the surface roughness. Also, the denser structure with lower porosity is obtained [50]. Additionally, the results in Table 2 show the increasing macrovoids in the membrane structure by increasing porosity from 68% in pristine membrane to 76% for PES-0.1 wt% CuO blended membrane. Moreover, at high concentration of CuO NPs (from 0.5 to 2 wt%), the mean pore size reduces; that is due to pore blockage [51] which leads to decrease of porosity from 76% in 0.1 wt% to 64% in 2 wt% NPs.

The SOM images were applied to show the distribution of NPs on the surface of fabricated membranes. As shown in Fig. 3, the uniform distribution of CuO NPs is clear for M2 to M5. But by increasing CuO concentrations, the nanoparticles tend to accumulate and cannot be properly distributed on the membrane surface (M6) [50].

To evaluate the morphology of the membrane surface, three-dimensional surface images were used. 3D images for membrane surface are shown in Fig. 4. According to the results (Table 3), the average surface roughness obtained was 8.23 nm for neat membrane, which increased by incorporation of CuO NPs for M2 and M3. The increase of surface roughness is the result of increase in membrane heterogeneity due to the presence of NPs into the membrane matrix. The low density and hydrophilic property of NPs causes their locating on the membrane surface. For M4 and M5, it is observed that R_a decreased and the surface of the membranes was smoother. This phenomenon can be the result of the uniform distribution of NPs at the surface of the membranes, which results in the filling of the surface cavities, by NPs. But at high concentration of CuO NPs (M6), surface roughness increased again due to aggregation and collapse of NPs. Accumulation of NPs at high concentrations is one of the most important reasons for the roughness and heterogeneity of membrane surface [45,52,53].

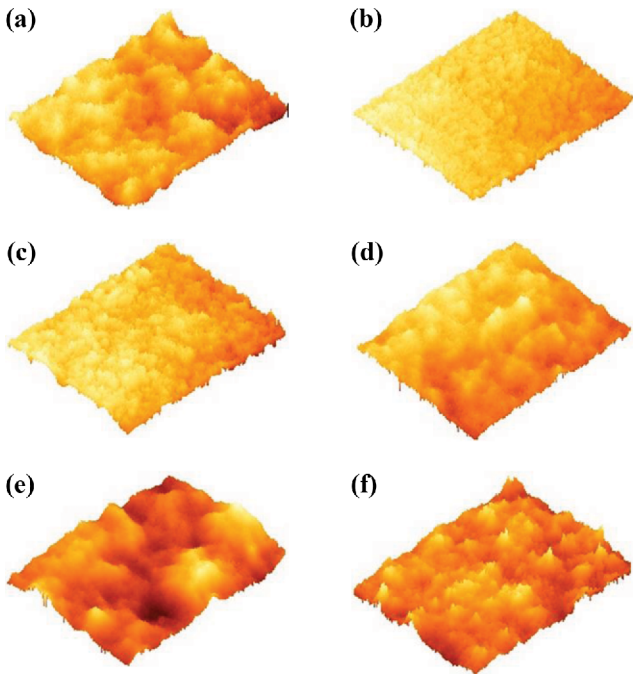

Fig. 4. The 3D surface images and average roughness (R_a) for the prepared membranes (a) M1, (b) M2, (c) M3, (d) M4, (e) M5, (f) M6.

Table 3. The average surface roughness for the fabricated membranes

Membrane	Average roughness (nm)
M1-pristine membrane	8.23
M2-0.05 wt% NP	8.76
M3-0.1 wt% NP	9.93
M4-0.5 wt% NP	6.76
M5-1 wt% NP	7.10
M6-2 wt% NP	10.26

2. Membrane Mechanical Strength

The measurements of membrane tensile strength were used to investigate the membrane mechanical properties. The obtained results are shown in Fig. 5. As is clear in Fig. 5, by increase of CuO NP concentration up to 0.1 wt% in the polymeric solution, membrane tensile strength was reduced. Because the amount of pores increased in the membrane structure by increasing CuO NPs, that decreases the tensile strength of membrane. Furthermore, the increase of porosity and channels into the membrane structure leads to an unstable and loose structure for these membranes [54,55].

The obtained results indicate that tensile strength was enhanced by increasing CuO NPs loadings into the PES (M4 and M5). Formation of strong interfacial bonding between nanoparticles and polymer has a high effect on the enhancement of the mechanical strength. Moreover, the embedding CuO NPs into the PES as membrane matrix leads to physical cross-linking into membrane structure that enhances internal membrane connections, leading to an increase of rigidity. Decreasing mechanical tensile strength in M6 compared to M5 is due to agglomeration and accumulation of particles in the high loading of nanoparticles, which led to rupture of the membrane structure and reduction of tensile strength.

3. Membrane Contact Angle

Generally, the hydrophilicity on the surface of membrane has a

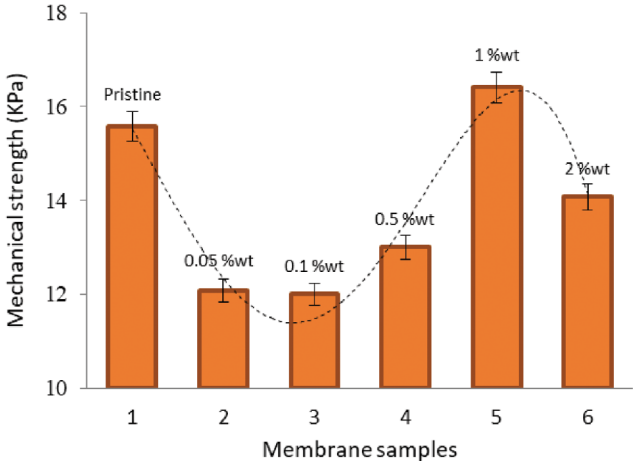

Fig. 5. The alterations of mechanical tensile strength with CuO nanoparticle concentration for all fabricated membranes.

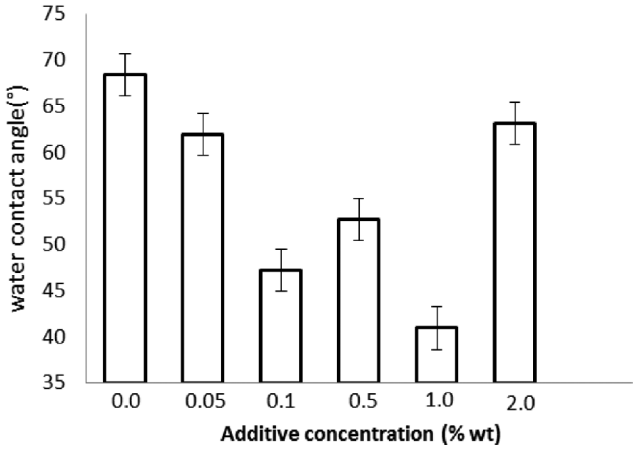

Fig. 6. The effect of CuO nanoparticles loading on the membrane contact angle.

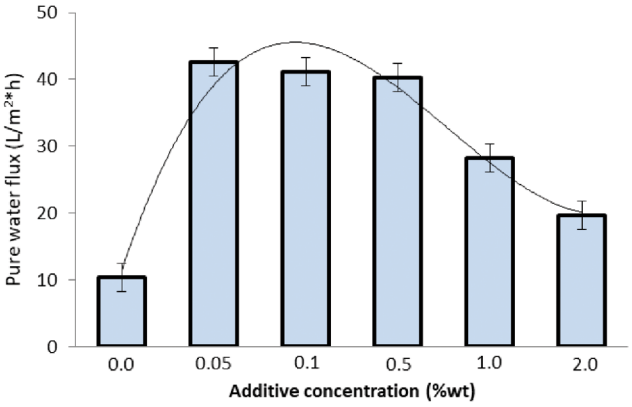

Fig. 8. The pure water flux for the prepared membranes with various concentrations of copper oxide nanoparticles.

reverse relationship with the contact angle on the membrane surface, and the smaller contact angle shows a higher hydrophilicity surface. The more hydrophilic surface prevents the deposition of pollutants and suspended particles at the surface of the membrane. Indeed, because of the presence of more water molecules on the surface of membrane during the separation process, the membrane anti-fouling properties are also strengthened. The measured contact angles for all fabricated membranes are shown in Fig. 6. The results show that the largest contact angle was obtained to M1; that is due to PES hydrophobic structure. After introducing CuO NPs into the membrane matrix, by reduction of contact angle, a growth in membrane hydrophilicity resulted. The migration of CuO NPs on the surface of membrane enhances the hydrophilicity of membrane compared to the unmodified PES membrane [6,56]. The increase of contact angle at high additive concentration creates rougher membrane surface and leads to nanoparticle agglomeration. As mentioned, an important factor that strongly controls the antifouling ability of composite membranes is the surface hydrophilicity of membrane.

4. Membrane Water Content

Another parameter for measurement of membrane hydrophilicity is water content. Fig. 7 shows the results of membrane water content. Incorporation of CuO NPs in membrane preparation led to increase in water content from 69% for the neat membrane to 71.8% for the modified membrane at 0.5 wt% NPs. The improvement of water content depends on the hydrophilic properties of CuO NPs. The interaction of CuO NPs and polymer into the casting solution decreased the polymeric chain interactions. Thus, the exchange rate between solvent and water occurred faster and led to increase voids and their size into the membrane structure and thus water content. As shown in Table 2, at high loadings of CuO nanoparticles from 0.5 to 2 wt%, water content decreased from 71.8% to 65.2% because of the agglomeration of NPs and the reduction of pore size [57].

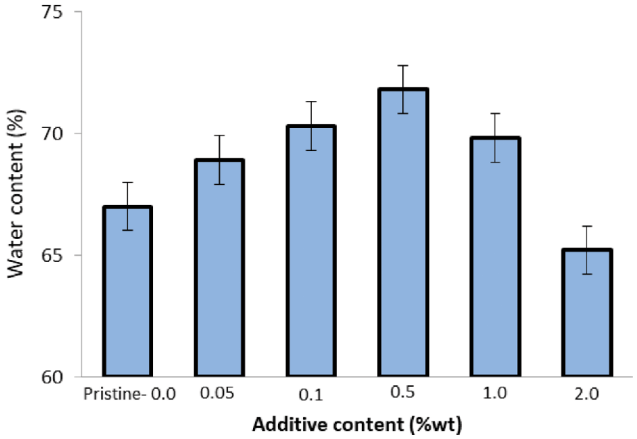

Fig. 7. The water content of pristine and mixed matrix membranes.

5. Membrane Separation Performance

5-1. Water Permeability

The results of the PWF for fabricated membranes are shown in Fig. 8. The increasing the PWF is under the influence of two major parameters: membrane hydrophilicity and membrane morphology. The presence of CuO NPs as hydrophilic NPs increased membrane hydrophilicity and leads to increase in water flow through the membrane. Moreover, the membrane morphology and the properties of membrane structure, such as increasing the porosity, enhancing the average pore size, reducing the thickness of the top-layer and improving the shape of the membrane channels, affect pure water flux. According to the results, the use of copper oxide hydrophilic NPs into the membrane structure increased the penetration rate of water into the polymer film, as well as increasing the velocity of penetration of solvent from the membrane into the water; empty spaces and cavities form into the membrane structure, which will improve the flux. On the other hand, according to Fig. 6, the water contact angle reduces by increasing CuO NPs, indicating the improvement of hydrophilicity and thus pure water flux. The increase of PWF is very impressive for samples M2 (42.63 L/m^2h) to M4 (40.27 L/m^2h) compared to the neat membrane (10.41 L/m^2h). By increasing the NPs concentration of to 2 wt% (M6) decreased pure water flux to 19.72 L/m^2h. Because the viscosity of the polymeric solution increased and the phase inversion rate decreased (as clear in Fig. 2), also increasing the thickness of top layer acted as a resistance layer against water molecules trans-

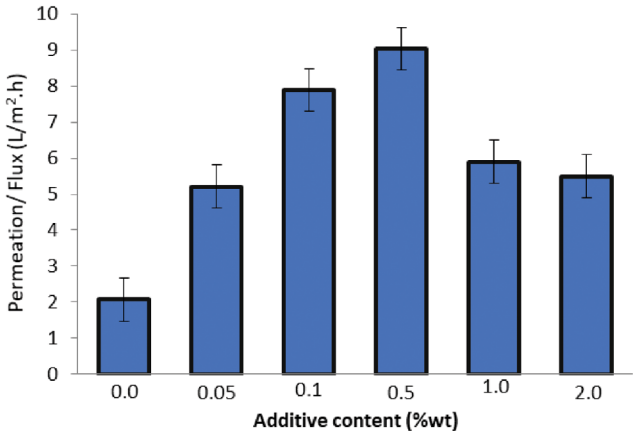

Fig. 9. Influence of CuO nanoparticle ratios on permeability of fabricated membranes.

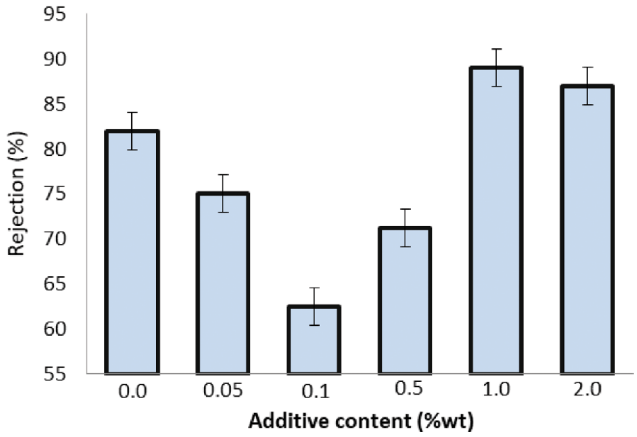

Fig. 10. The change of salt rejection with CuO nanoparticle loading for membranes.

port. Furthermore, the tendency of NPs to accumulate and aggregate causes the blockage of membrane cavities which reduces porosity and pore size [1,44,58,59]. Note that despite reducing flux at higher concentrations of CuO NPs, the obtained flux for MMMs is more than the neat membrane, which indicates the desired effects of CuO NPs on the PWF.

5-2. Salt Rejection

Salt rejection and membrane permeability were determined to study the performance of the prepared MMMs compared to the unmodified membrane. Fig. 9 illustrates the effect of nanoparticle loading on the membrane permeation/flux. As is clear in Fig. 9, permeability improved from M1 (pristine membrane) to M4 (0.5 wt% of CuO NPs). The main factor for the improvement of solute flux is the synergetic effect among water molecules and hydrophilic CuO NPs on the membrane surface.

Suitable concentration of NPs in casting solution led to the increment in the exchange rate between solvent and non-solvent and their good dispersion. Thus porosity increased into the membrane structure (see Fig. 2). Incorporation of higher concentration of CuO NPs into the membrane solution (M5 and M6) restricted flux due to increase casting solution viscosity and macrovoid elimination. Moreover, the agglomeration of CuO NPs at high concentrations and pore blockage resulted in the reduction of solute flux. By reducing pore size of cavities, smaller pathway for water transport through the membrane was created [44,60].

As is clear in Fig. 10, the rate of rejection decreased by adding CuO NPs from 82% in M1 (pristine membrane) to 62.5% in M3 (at 0.1 wt% of CuO NPs). Because porosity increased from M1 to M3 (see Table 2), that facilitated solute transport through the membrane. Furthermore, by increasing membrane surface roughness and the agglomeration of undesirable particles in the surface of membrane increases the possibility of passing salt ions from the membrane. But the salt rejection was enhanced from M3 at 0.1 wt% CuO NPs (62.5%) to M5 at 1 wt% CuO NPs (89%) due to filling porosities by CuO NPs and the formation of smoother and denser surface (according to Fig. 2 and Fig. 4). Also, increasing the selective layer thickness enhanced the membrane resistance against ion transport and increased salt rejection. The electrostatic repulsion mechanism between hydroxyl groups on the nanoparticle surface and SO_4^{2-} ions is another reason for promotion of salt rejection [61,62].

Subsequently, by the increment of the nanoparticle concentration to 2 wt%, the rejection rate was reduced slightly. The phenomenon of nanoparticles agglomeration, reducing the effective surface of NPs and filling the membrane pores by NPs led to decrease active sites for salt adsorption on the membrane surface [29,52,63].

6. Membrane Antifouling Performance

The filtration of powder milk solution (8,000 mg/L) and then pure water were used to analyze and evaluate the antifouling performance of prepared membranes. Obtained results showed that the MMMs have better antifouling properties than pristine membrane which was examined by FRR% as a main fouling factor. FRR% improved from ~63% for the neat membrane to 77-93% for MMMs. The highest FRR% was measured ~93% for M5 (1 wt% CuO NPs). The enhancement of membrane surface hydrophilicity is the main reason for increasing FRR%. This improves the molecular water movement on their surface. Also, the absorption of water molecules increases on a hydrophilic surface, which forms a thin layer of water that acts as barrier for powder milk solution transport through the membrane [34,64]. Some decrease in FRR% at high additive concentrations can be justified by agglomeration of CuO NPs on the membrane surface.

CONCLUSION

Hydrophilic CuO NPs were used to fabricate MMMs. The influence of various loading of CuO NPs was used to investigate fouling resistance and separation performance of NF membranes. SEM images indicated the formation of a dense superficial layer and a porous substrate with finger-like structure. SOM images also indicated the almost uniform distribution of nanoparticles on the membrane surface. The surface analysis indicated which of the rougher membranes was obtained by increasing additive content at first, then decrease. Moreover, in 2 wt% CuO NPs for M6, average roughness reached the highest value. Porosity, mean pore size, water content, and water flux and membrane tensile strength were improved

by embedding CuO NPs. The highest pure water flux was observed for M2 (42.63 L/m^{2}h) to M4 (40.27 L/m^{2}h), which indicated a four-times increase compared to the neat membrane (10.41 L/m^{2}h). The highest salt rejection (89%) was obtained to M5 at 1 wt% of CuO NPs, while the salt rejection of pristine membrane measured 82%. The MMMs showed significant antifouling properties with FRR% (~77% to ~93%), whereas that was ~63% for the pristine membrane.

ACKNOWLEDGEMENT

Authors gratefully acknowledge Arak University for the financial support during this research.

REFERENCES

1. B. Al-Rashdi, D. Johnson and N. Hilal, *Desalination*, **315**, 2 (2013).
2. C. Bellona, in *Desalination: water from water*, J. Kucera Ed., Wiley, Beverly, MA (2014).
3. Y. Han, Z. Xu and C. Gao, *Adv. Funct. Mater.*, **23**, 3693 (2013).
4. G. Abdi, A. Alizadeh, S. Zinadini and G. Moradi, *J. Membr. Sci.*, **552**, 326 (2018).
5. S. Bandehali, A. Kargari, A. Moghadassi, H. Saneepur and D. Ghanbari, *Asia-Pac. J. Chem. Eng.*, **9**, 638 (2014).
6. S. Ansari, E. Bagheripour, A. Moghadassi and S. M. Hosseini, *J. Polym. Eng.*, **37**, 61 (2017).
7. E. Bagheripour, A. Moghadassi and S. Hosseini, *Arab. J. Sci. Eng.*, **41**, 2545 (2016).
8. M. Farjami, A. Moghadassi, V. Vatanpour, S. M. Hosseini and F. Parvizian, *J. Ind. Eng. Chem.*, **72**, 144 (2018).
9. A. Gholami, A. Moghadassi, S. Hosseini, S. Shabani and F. Gholami, *J. Ind. Eng. Chem.*, **20**, 1517 (2014).
10. E. Bagheripour, A. Moghadassi and S. Hosseini, *Int. J. Eng.*, **29**, 280 (2016).
11. N. Hilal, H. Al-Zoubi, N. A. Darwish, A. W. Mohamma and M. Abu Arabi, *Desalination*, **170**, 281 (2004).
12. N. Nasrollahi, S. Aber, V. Vatanpour and N. M. Mahmoodi, *COMPOS PART B-ENG*, **154**, 388 (2018).
13. H. Sanaeepur, A. E. Amooghin, S. Bandehali, A. Moghadassi, T. Matsuura and B. Van der Bruggen, *Prog. Polym. Sci.*, **91**, 80 (2019).
14. N. Nasrollahi, V. Vatanpour, S. Aber and N. M. Mahmoodi, *Sep. Purif. Technol.*, **192**, 369 (2018).
15. L. Gzara, Z. A. Rehan, S. B. Khan, K. A. Alamry, M. H. Albeirutty, M. El-Shahawi, M. I. Rashid, A. Figoli, E. Drioli and A. M. Asiri, *J. Taiwan Inst. Chem. E.*, **65**, 405 (2016).
16. N. Nasrollahi, S. Aber, V. Vatanpour and N. M. J. Mahmoodi, *Mater. Chem. Phys.*, **222**, 338 (2019).
17. S. Ayyaru and Y.-H. Ahn, *J. Ind. Eng. Chem.*, **67**, 199 (2018).
18. H. Rajabi, N. Ghaemi, S. S. Madaeni, P. Daraei, B. Astinchap, S. Zinadini and S. H. Razavizadeh, *Appl. Surf. Sci.*, **349**, 66 (2015).
19. T. D. Dipheko, K. P. Matabola, K. Kotlhao, R. M. Moutloali and M. Klink, *Int. J. Polym. Sci.*, **2017**, 8 (2017).
20. B. Van der Bruggen, *J. Appl. Polym. Sci.*, **114**, 630 (2009).
21. A. Sotto, A. Boromand, R. Zhang, P. Luis, J. M. Arsuaga, J. Kim and B. Van der Bruggen, *J. Colloid Interface Sci.*, **363**, 540 (2011).
22. H. Sanaeepur, A. Ebadi Amooghin and S. Bandehali, *Theoretical gas permeation models for mixed matrix membranes*, LAP LAMBERT Academic Publishing, Beau Bassin, Mauritius (2018).
23. A. Anand, B. Unnikrishnan, S.-C. Wei, C. P. Chou, L.-Z. Zhang and C.-C. Huang, *Nanoscale Horiz.*, **4**, 117 (2019).
24. S. Dervin, D. D. Dionysiou and S. C. Pillai, *Nanoscale*, **8**, 15115 (2016).
25. C. Zhao, B. Yang, J. Han, Y. Meng, L. Yu, D. Hou, J. Wang, Y. Zhao, Y. Zhai and S. Wang, *Appl. Surf. Sci.*, **453**, 502 (2018).
26. S. Beisl, S. Monteiro, R. Santos, A. S. Figueiredo, M. G. Sánchez-Loredo, M. A. Lemos, F. Lemos, M. Minhalma and M. N. de Pinho, *Water Res.*, **149**, 225 (2018).
27. P. Zhang, J.-L. Gong, G.-M. Zeng, B. Song, H.-Y. Liu, S.-Y. Huan and J. Li, *Chemosphere*, **204**, 378 (2018).
28. M. Jyothi, V. Nayak, M. Padaki and R. G. Balakrishna, *J. Photochem. Photobiol., A.*, **339**, 89 (2017).
29. A. Ahmad, A. Abdulkarim, Z. M. Shafie and B. Ooi, *Desalination*, **403**, 53 (2017).
30. O. Mahlangu, R. Nackaerts, J. Thwala, B. Mamba and A. Verliefde, *J. Membr. Sci.*, **524**, 43 (2017).
31. M. Sianipar, S. H. Kim, F. Iskandar and I. G. Wenten, *RSC Adv.*, **7**, 51175 (2017).
32. N. Rakhshan and M. Pakizeh, *J. Ind. Eng. Chem.*, **34**, 51 (2016).
33. M. L. Masheane, L. N. Nthunya, S. P. Malinga, E. N. Nxumalo, B. B. Mamba and S. D. Mhlanga, *Sep. Purif. Technol.*, **184**, 79 (2017).
34. S. M. Hosseini, M. Afshari, A. R. Fazlali, S. Koudzari Farahani, S. Bandehali, B. van der Bruggen and E. Bagheripour, *Chem. Eng. Res. Des.*, **147**, 390 (2019).
35. S. Madaeni, S. Zinadini and V. Vatanpour, *J. Membr. Sci.*, **380**, 155 (2011).
36. M. Baghbanzadeh, D. Rana, T. Matsuura and C. Q. Lan, *Desalination*, **369**, 75 (2015).
37. S. Hosseini, N. Rafiei, A. Salabat and A. Ahmadi, *Arab. J. Chem.*, **13**, 2470 (2020).
38. N. Ghaemi, S. S. Madaeni, P. Daraei, H. Rajabi, S. Zinadini, A. Alizadeh, R. Heydari, M. Beygzadeh and S. Ghouzivand, *Chem. Eng. J.*, **263**, 101 (2015).
39. P. Daraei, S. S. Madaeni, N. Ghaemi, H. A. Monfared and M. A. Khadivi, *Sep. Purif. Technol.*, **104**, 32 (2013).
40. E. Bagheripour, A. R. Moghadassi, S. M. Hosseini and M. Nemati, *JMSR*, **2**, 14 (2016).
41. S. Zinadini, A. A. Zinatizadeh, M. Rahimi, V. Vatanpour and H. Zangeneh, *J. Membr. Sci.*, **453**, 292 (2014).
42. P. Mobarakabad, A. Moghadassi and S. Hosseini, *Desalination*, **365**, 227 (2015).
43. E. Bagheripour, A. Moghadassi, S. Hosseini, M. Ray, F. Parvizian and B. van der Bruggen, *Chem. Eng. Res. Des.*, **132**, 812 (2018).
44. E. Bagheripour, A. R. Moghadassi, F. Parvizian, S. M. Hosseini and B. van der Bruggen, *Chem. Eng. Res. Des.*, **144**, 418 (2019).
45. S. Hosseini, E. Bagheripour, A. Hamidi, A. Moghadassi and S. Madaeni, *J. Iran Chem. Soc.*, **13**, 1749 (2016).
46. D. Emadzadeh, M. Ghanbari, W. Lau, M. Rahbari-Sisakht, D. Rana, T. Matsuura, B. Kruczek and A. Ismail, *Mater. Sci. Eng. C*, **75**, 463 (2017).
47. F. S. Halek, S. K. Farahani and S. M. Hosseini, *Korean J. Chem. Eng.*, **33**, 629 (2016).
48. M. K. Clark Wooten, V. R. Koganti, S. Zhou, S. E. Rankin and B. L.

Knutson, *ACS Appl. Mater. Interfaces*, **8**, 21806 (2016).
49. X. Chen, M. Qiu, H. Ding, K. Fu and Y. Fan, *Nanoscale*, **8**, 5696 (2016).
50. S. M. Hosseini, E. Bagheripour and M. Ansari, *Korean J. Chem. Eng.*, **34**, 1774 (2017).
51. S. Hosseini, S. Madaeni and A. Khodabakhshi, *Sep. Sci. Technol.*, **47**, 455 (2012).
52. M. Moochani, A. Moghadassi, S. M. Hosseini, E. Bagheripour and F. Parvizian, *J. Chem. Eng.*, **33**, 2674 (2016).
53. M. R. Mehrnia, Y. M. Mojtahedi and M. Homayoonfal, *Desalination*, **372**, 75 (2015).
54. S. M. Hosseini, P. Koranian, A. Gholami, S. S. Madaeni, A. R. Moghadassi, P. Sakinejad and A. R. Khodabakhshi, *Desalination*, **329**, 62 (2013).
55. S. M. Hosseini, A. Hamidi, A. Moghadassi and S. S. Madaeni, *Korean J. Chem. Eng.*, **32**, 429 (2015).
56. S. Hosseini, E. Jashni, M. Jafari, B. Van der Bruggen and Z. Shahedi, *J. Membr. Sci.*, **560**, 1 (2018).
57. M. Amirilargani, M. Sadrzadeh, E. J. R. Sudhölter, L. C. P. M. de Smet, *Chem. Eng. J.*, **289**, 562 (2016).
58. X. Wei, X. Xu, J. Wu, C. Li, J. Chen, B. Lv, B. Zhu and H. Xiang, *J. Appl. Polym. Sci.*, **136**, 47436 (2019).
59. H. Zangeneh, A. A. Zinatizadeh, S. Zinadini, M. Feyzi and D. W. Bahnemann, *Sep. Purif. Technol.*, **209**, 764 (2019).
60. S. Abdikheibari, W. Lei, L.F. Dumée, N. Milne and K. Baskaran, *J. Mater. Chem.*, **6**, 12066 (2018).
61. Y. He, Y. P. Tang and T. S. Chung, *Ind. Eng. Chem. Res.*, **55**, 12929 (2016).
62. R. W. Baker, *Membrane technology and applications*, 3th Ed., Wiley, U.K. (2012).
63. S. Bano, A. Mahmood, S.-J. Kim and K.-H. Lee, *J. Mater. Chem. A.*, **3**, 2065 (2015).
64. M. Akhond and J. Tashkhourian, *Bull. Korean Chem. Soc.*, **24**, 489 (2003).